

Online Ensemble Transformer for Accurate Cloud Workload Forecasting in Predictive Auto-Scaling

Jiadong Chen
Shanghai Jiao Tong Univ.
Shanghai, China

Xiao He
ByteDance Inc.
Hangzhou, China

Hengyu Ye
Shanghai Jiao Tong Univ.
Shanghai, China

Fuxin Jiang
ByteDance Inc.
Beijing, China

Tieying Zhang
ByteDance Inc.
San Jose, USA

Jianjun Chen
ByteDance Inc.
San Jose, USA

Xiaofeng Gao
Shanghai Jiao Tong Univ.
Shanghai, China

ABSTRACT

In the swiftly evolving domain of cloud computing, the advent of serverless systems underscores the crucial need for predictive auto-scaling systems. This necessity arises to ensure optimal resource allocation and maintain operational efficiency in inherently volatile environments. At the core of a predictive auto-scaling system is the workload forecasting model. Existing forecasting models struggle to quickly adapt to the dynamics in online workload streams and have difficulty capturing the complex periodicity brought by fine-grained, high-frequency forecasting tasks. Addressing this, we propose a novel online ensemble model, E^3 Former, for online workload forecasting in large-scale predictive auto-scaling. Our model synergizes the predictive capabilities of multiple subnetworks to surmount the limitations of single-model approaches, thus ensuring superior accuracy and robustness. Remarkably, it accomplishes this with a minimal increase in computational overhead, adhering to the lean operational ethos of serverless systems. Through extensive experimentation on real-world workload datasets, we establish the efficacy of our ensemble model. In online forecasting tasks, the proposed method reduces forecast error by an average of 10%, and its effectiveness is further demonstrated through a predictive auto-scaling test in the real-life online system. Currently, our method has been deployed within ByteDance’s Intelligent Horizontal Pod Auto-scaling (IHPA) platform, which supports the stable operation of over 30 applications, such as Douyin E-Commerce, TouTiao, and Volcano Engine. The predictive auto-scaling capacity reaching over 600,000 CPU cores. On the basis of essentially ensuring service quality, the predictive auto-scaling system can reduce resource utilization by over 40%.

could lead to: Under-provisioning causes the system to overload, while over-provisioning incurs unnecessary resource costs [25].

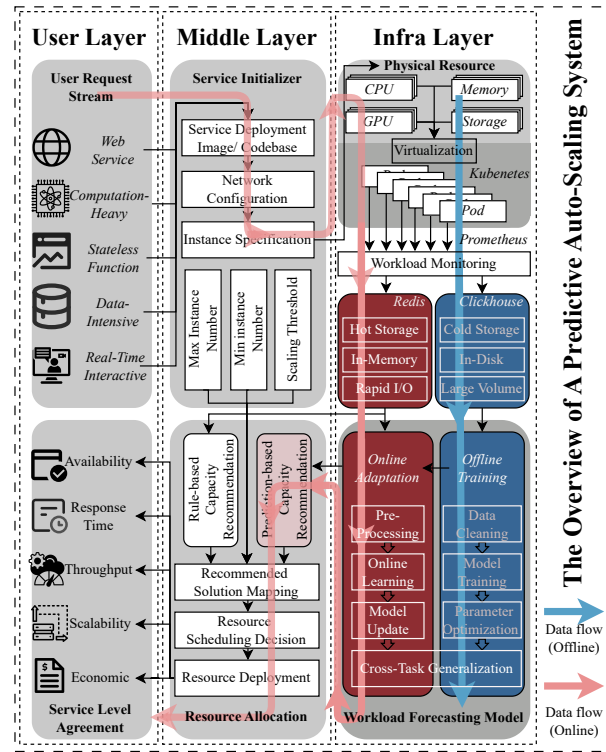


Figure 1: The overview of a predictive auto-scaling systems, which is divided into three layers: User Layer, Middle Layer, and Infra Layer. The system integrates predictive analytics to achieve proactive scaling decisions by a workload forecasting model. The workload forecasting model combines offline training with online adapting to help system optimize resource allocation, ensuring scalability, cost-efficiency, and adherence to service-level agreements.

1 INTRODUCTION

Modern cloud computing systems rely on elastic auto-scaling mechanisms to dynamically allocate physical resources, balancing cost efficiency and service quality. At the core of this capability lies workload forecasting, a technique that predicts future resource demands to guide scaling decisions [14, 16, 32], as shown in Figure 1. Research has demonstrated that elaborate auto-scaling systems with accurate workload forecasting can enhance service quality by 20% while reducing resource waste by 15% [13]. However, to achieve the goal of cost reduction and efficiency improvement, forecasting models need to be versatile and capable of addressing a variety of challenges. Figure 2 shows the results that an inadequate forecast

Cloud system workloads exhibit four distinct characteristics that complicate forecasting. **1) Complex periodic patterns** arise from multi-scale cycles (e.g., hourly, daily, weekly, and seasonal variations) intertwined with irregular bursts, as shown in Figure 3. **2) Long-term prediction length** (ranging from minutes to hours) are essential due to the latency of physical resource allocation

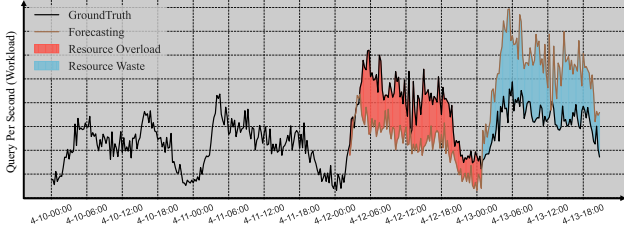


Figure 2: When the predicted value exceeds the actual workload (blue zone), it not only wastes physical resources but also incurs unnecessary costs¹. Conversely, underestimating the workload (red zone) can lead to system overload and a decrease in service quality.

in data centers. **3) Changing dynamics** arise from either user behaviors or system updates, which necessitate that the forecasting model must be capable of online adaptation. **4) Robustness** is of paramount importance, as cloud computing systems must ensure Service Level Agreements (SLAs). Therefore, as the core of the auto-scaling system, the forecasting model must be capable of handling diverse sequences and generating robust predictions.

To address these limitations, we present an online workload forecasting model comprising four synergistic components: **1) Representer:** Extracts multi-resolution periodic features through multi-resolution patching operation, explicitly modeling nested cycles. **2) Transformer:** Leverages self-attention modules to capture long-range dependencies. **3) Adapter:** Implements online adaptation via cumulative gradient-based parameters updates, enabling rapid refining to workload dynamics. **4) Ensemble:** Combines results from different sub-networks through adaptive weighting, enhancing robustness against distribution shifts.

We also collect and open-source high-quality workload datasets² from distinct cloud service types in ByteDance Cloud, containing workload data of thousands of computing instances, spanning from 1 month to 2 months. We carefully preprocess the raw data, and make them useful tools for the community to evaluate and develop new workload forecasting methods. In online forecasting tasks on twelve datasets, compared with the previous SOTA, E³Former reduces forecast MSE/MAE/WMAPE by an average of **13.9%/11.7%/19.1%**. In transfer forecasting tasks that simulate real-world cold-start scenarios, E³Former shows generalization ability and robustness, and reduces forecast MSE/MAE/WMAPE by an average of **15.3%/14.1%/26.3%**. Moreover, to substantiate the practical applicability of our model, we implement it within a real-life online kubernetes system and carry out a predictive auto-scaling test. Compared with the built-in Naive HPA module in kubernetes, the scaling strategy based on E³Former reduces the average/maximum Pod occupation by **7.3%/29.4%** and decreases the system’s average/maximum latency by **5.6%/91.7%**. This study serves to confirm the model’s efficacy and highlights its utility in real-world scenarios, underlining its potential to enhance predictive accuracy and

¹For a distributed computing cluster comprising hundreds of thousands of CPU cores, every 1% of resource wastage translates to an annual revenue loss of tens of thousands, if not hundreds of thousands, of dollars.

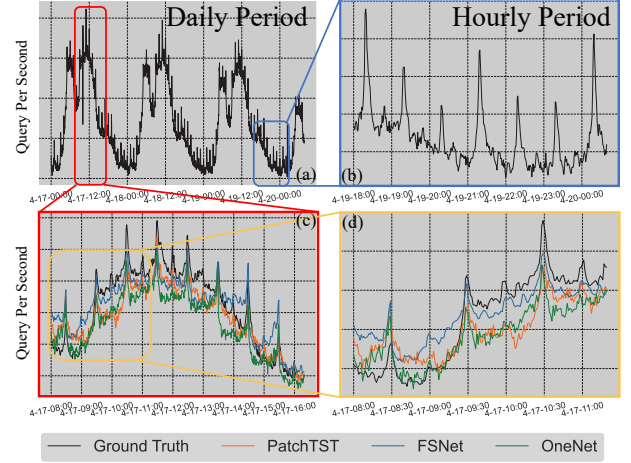


Figure 3: Workload shows multi-granularity periodic pattern, and recent works cannot capture such complicated dynamics.

operational efficiency in diverse applications. Our contributions are summarized as follows:

- (1) To address the challenges of online workload forecasting, we design the Representer to extract multi-granularity periodic patterns, the Adapter to achieve rapid online updates at parameter level, and the Ensemble to improve robustness with online learning theory.
- (2) We develop an efficient and effective Transformer-based ensemble framework, achieving significantly more accurate results with a negligible increase in parameters.
- (3) We collect and open-source workload datasets from real-world large-scale cloud systems, and conduct comprehensive experiments on them, showcasing the superiority of our proposed model over typical baselines.
- (4) In Kubernetes HPA proactive auto-scaling tests, compared with the built-in Naive HPA module, E³Former reduces the average / maximum latency by 5.6% / 91.7% and the average / maximum resource consumption by 7.3% / 29.4%.

2 RELATED WORKS

Predictive Auto-Scaling. Auto-scaling has emerged as a pivotal mechanism for the efficient allocation and relinquishment of resources in accordance with workload variations [3], resulting in significant reductions in operational and management expenses [33]. Proactive auto-scaling based on time series forecasting can prepare resources in advance to ensure Quality of Service (QoS) during peak load periods, and reduce resources promptly during low load periods to avoid resource wastage [14, 32]. Zhou et al. propose AHPA [44], a robust decomposition-based statistical method for predicting resource load in services, subsequently enabling horizontal scaling of pods based on expected resource demands. Guo et al. introduce PASS [13], which employs a prediction framework that integrates both online and offline prediction models to enhance the accuracy of resource prediction, thereby achieving higher quality auto-scaling. Accurate forecasts play a vital role in such systems.

²<https://huggingface.co/datasets/ByteDance/CloudTimeSeriesData>

Workload Forecasting in Systems. In large-scale systems, workload modeling is usually done with statistical or machine learning methods [5, 8, 10, 17]. With the development of deep learning, state-of-the-art time series prediction techniques for workloads have begun to be applied to system load balancing, parameter optimization, capacity scaling, etc. LoadDynamics [21] employs a combination of LSTM and Bayesian optimization for handling the dynamic fluctuations of cloud workloads. Seagull [31] is an end-to-end generic ML infrastructure for load prediction and optimized resource allocation by adjusting plugged ML models. WGAN-gp Transformer [2] adopts a Transformer network as a generator and a multi-layer perception as a critic to predict cloud workload. QueryBot [28] combines linear regression and RNNs for various database workload patterns. DBAugur [11] uses adversarial neural networks to predict the trends of database workloads and shows the superiority of index selection and data region migration tasks.

Table 1: Workload Metrics by Architecture Layers.

Service Layer	Network			App Service
Throughput & Reliability	In-Traffic Latency	Out-Traffic UDP Loss	TCP Conn. Packet Rate	Requests Resp. Time
System Layer	Database		OS	
Performance & Latency	Conn. Count Query Time	Cache Hit Index Usage	Waiting Procs Context Switches	Running Procs Load
Infra Layer	CPU		Memory	Storage
Core Metrics & Health	Total Usage Temperature	Core Load Frequency	Usage Swap Rate	Disk I/O Remaining

3 PRELIMINARIES

3.1 Workload Data Stream

In the context of cloud computing, a workload series represents a time-ordered aggregation of workloads generated by jobs or applications operating on cloud infrastructure [1]. Table 1 concludes common types of workload in cloud environment, including distinct resource-consumption patterns (such as CPU and memory usage) and user-request metrics (like response time). In online scenarios, the workloads appear as potentially unbounded streams of continuous data in real (or near-real) time, reflecting system statuses, as described in Def. 1.

DEFINITION 1 (WORKLOAD STREAM). *A workload stream, or an kind of online time series, is a sequence of signals (such as CPU usage, memory usage, etc.), measured at successive time stamps, which are assumed to be spaced at uniform intervals (such as every minute). We denote by x_t the signal recorded at time stamp t , and a data stream can be denoted as $\mathbf{X} = \{x_1, x_2, \dots, x_t, \dots\}$.*

With the operation of the large-scale system, new workload metrics are continuously recorded, and the stream is continuously longer. Due to the need for real-time and efficiency, we cannot use unlimited memory and storage to record all histories and then predict the future. As shown in Figure 1, online workload streams are stored in two forms: cold storage and hot storage. Cold storage uses hard disks as the storage medium and is managed through OLAP

databases such as ClickHouse. It can store large-scale workload data on a monthly basis, but its read speed is limited, making it unsuitable for real-time analysis tasks. Hot storage, on the other hand, uses memory as the storage medium and is managed through in-memory databases such as Redis. Its read and write speeds are highly efficient, supporting real-time analysis. However, due to capacity constraints, it can only store a limited amount of data, such as workload from the past week.

Given the limited historical data accessible in online environments, which is insufficient for complete offline training, a pipeline combining offline pretraining with online updating is more suitable. The model initially learns from large-scale historical data and then adapts to the online environment based on the limited available data to generate accurate and efficient predictions.

3.2 Online Workload Forecasting

Firstly, there is no separation of training and evaluation in an online setting. Instead, learning occurs over a sequence of time-steps [30]. Hence, At each time stamp t , we can define a length parameter L and use observation history $\mathbf{X}_t = \{x_{t-L}, x_{t-L+1}, \dots, x_{t-1}\} = \{\mathbf{x}\}_{t-L}^{t-1}$, where $\mathbf{x}_t \in \mathbb{R}^M$ denotes the M kinds of workload metrics recorded at time t , to produce a H -length prediction $\hat{\mathbf{Y}}_t = f(\mathbf{X}_t; \theta_t^f) = \{\hat{x}_L, \hat{x}_{L+1}, \dots, \hat{x}_{L+T-1}\}$ with prediction model f and associated parameter set θ_t^f . \mathbf{X}_t is a fixed-length observed series history, focusing on the latest and limited observation in online scenarios.

We use loss function $\ell(\hat{\mathbf{Y}}_t, \mathbf{Y}_t)$ to measure the gap between the prediction $\hat{\mathbf{Y}}_t$ and truth \mathbf{Y}_t . Specifically, ℓ maps the prediction and the truth into a real number in $[0, 1]$, and the more accurate the prediction is, the smaller the loss is. Depending on the requirements, there are many choices of ℓ .

Secondly, since a data stream is recorded continuously, we notice that the learning parameter θ should be updated at each time t , which derives the formal definition of OnPred, denoted as Def. 2.

DEFINITION 2 (ONLINE WORKLOAD FORECASTING). *At time stamp t , given an L -length history stream \mathbf{X}_t , the online workload forecasting task requires a prediction $\hat{\mathbf{Y}}_t^f = f(\mathbf{X}_t; \theta_t^f)$. After making the prediction, the prediction model f then receives the true answer \mathbf{Y}_t and generates a related loss $\ell(\hat{\mathbf{Y}}_t, \mathbf{Y}_t)$. Whenever the loss is nonzero, f updates the parameter set from θ_t^f to θ_{t+1}^f by applying some update strategy on the training example pair $(\mathbf{X}_t, \mathbf{Y}_t)$. By running the online learning T time-steps, the goal of online workload forecasting is to minimize the cumulative loss, i.e., $\sum_{t=1}^T \ell(\hat{\mathbf{Y}}_t, \mathbf{Y}_t)$.*

PROCEED [41] proposes the view that an online learning task inherently has a H -step feedback delay in time series forecasting, resulting in a temporal gap (at least H steps) between available training samples and the test sample. In practical workload forecasting tasks, there is typically a certain interval between two consecutive predictions, as repeated predictions would lead to resource waste. Ideally, this interval should be set to the length of the forecast horizon to meet the needs of guiding scaling operations. Therefore, the online forecasting setting is immune to this temporal gap.

In general, the performance of an online model is measured by comparing its cumulative loss with the minimum cumulative loss

Table 2: Symbols and Notations

Symbols	Definitions
\mathbf{X}	workload data stream
\mathbf{x}_t	workload series point at timestamp t
M	number of metrics of the workload stream
L	lookback length
H	forecasting length
$\mathbf{X}_t, \mathbf{Y}_t$	input and output series at time t
$\hat{\mathbf{Y}}_t = f(\mathbf{X}_t; \theta_t^f)$	forecasting with input \mathbf{X}_t and parameter θ_t^f
P	patch size
D, D', D_{ff}	hidden dimension of different modules
W^O, W^Q, W^K, W^V	learnable parameter matrices
∇	cumulative gradient
α, β	adaptation coefficients
Δ, Π	decision space for model ensemble
\mathbf{w}, π	decision strategy for model ensemble

of the offline algorithm, and its difference is denoted as *regret* [18]:

$$\text{regret} = \sum_{t=1}^T \ell(f(\mathbf{X}_t; \theta_t^f), \mathbf{x}_t) - \inf_{\theta} \sum_{t=1}^T \ell(f(\mathbf{X}_t; \theta), \mathbf{x}_t). \quad (1)$$

The second term in Eqn. (1) is the loss suffered by the model with the best parameter setting θ^* , which can only be known in hindsight after seeing the full data stream. An online model's regret is *sub-linear* as a function of T , if and only if $\text{regret} = o(T)$, which implies $\lim_{T \rightarrow \infty} \frac{\text{regret}}{T} \rightarrow 0$ and thus on average the model performs almost as well as setting the best parameter in hindsight. We always expect an online learner achieving a sub-linear regret. Table 2 presents the primary notations with the corresponding definitions.

4 MODEL DESIGN

In this section, we outline the methodologies designed to address the challenges in workload forecasting. To extract complex periodic patterns, we designed the Reresenter, which centers on a multi-resolution patching operation. To model long-term dependencies, we leverage a Transformer forecasting model. To capture changing dynamics, we design the Adapter module to achieve effective online parameter updates. To generate robust predictions, we design an Ensembler with two alternative ensemble modules (Online Scaling and Follow-The-Perturbed-Leader) based on online learning theory. Through the multi-resolution patching operation, the input is transformed into multiple sets of patches, retaining periodic information at various levels. These sets of patches are then fed into the parameter-shared Transformer to produce corresponding multiple outputs. During the offline training phase, each output is used independently to train the corresponding sub-networks. In the online inference phase, the Ensembler integrates these multiple outputs to generate the final prediction results. Meanwhile, the Adapter ensures the model fits the changing dynamics of the workload.

4.1 Representer

We designed the Representer module to extract multi-level periodic features from workload series and represent them in a form

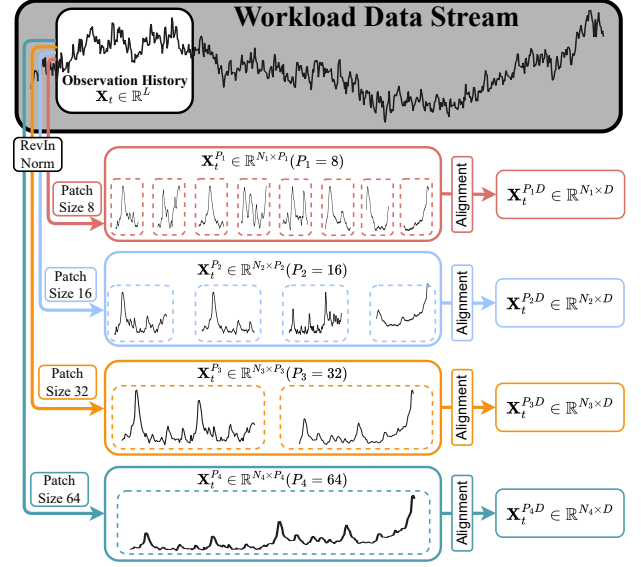


Figure 4: The pipline of Representer. Initially, the RevIN Norm technique is employed to regularize the data distribution of the input historical sequence. Subsequently, the sequence undergoes a patching operation using patches with different lengths (8, 16, 32, and 64), which segments the sequence into equal-length patches. Finally, a linear layer is utilized to map the last dimension of these patches to a uniform hidden layer dimension D , ensuring consistency for further processing in the model.

suitable for parallel processing. Specifically, the Representer has four operations: channel independence, RevIN, multi-resolution patching, and alignment.

4.1.1 Channel Independence. In channel independence setting [29], each channel of a multivariate time series is treated as independent. Specifically, the multivariate time series $\mathbf{X}_t \in \mathbb{R}^{L \times M}$ is organized as a M -sized mini-batch of single-variate time series $\{\mathbf{X}_{t,i}\}_{i=1}^M$. Through channel independence, we can fully utilize the parallelism of GPUs, expand the training set by M times, and avoid overfitting caused by complex inter-channel relationships. Since each series in the minibatch goes through the same parallel pipeline, we abbreviate $\mathbf{X}_{t,i}$ as $\mathbf{X}_t \in \mathbb{R}^L$.

4.1.2 RevIN. Reversible Instance Normalization (RevIN) [23] is a normalization method for time series. It performs instance normalization by calculating the mean μ and standard deviation σ over \mathbf{X}_t . Then, it normalizes the data: $\hat{\mathbf{X}}_t = \frac{\mathbf{X}_t - \mu}{\sigma}$. Later, RevIN applies an affine transformation with learnable parameters r_1 and r_2 : $\hat{\mathbf{X}}_t = r_1 \hat{\mathbf{X}}_t + r_2$. During denormalization, the process is reversed to restore the original data distribution.

4.1.3 Multi-resolution patching. The patching operation can help extract the local periodic information from a series. Specifically, given the patch size P , the input time series $\hat{\mathbf{X}}_t$ can be divided into multiple P -sized patches $\mathbf{X}_t^P \in \mathbb{R}^{N \times P}$, where N is the number of patches calculated as $N = \lceil L/P \rceil$. To handle the end of the series, the last value of \mathbf{X}_t is padded with repeated numbers $(L \bmod P)$,

ensuring that each patch maintains consistent dimensions. Research shows that the patch-based projections with larger patch sizes can capture high-frequency features and vice versa [37]. Furthermore, in order to represent the periodic features of different levels, we design a multilevel patching method. We utilize a group of different patch sizes $\{P_1, \dots, P_d\}$ and process the input time series into multiple groups of patches $\{X_t^{P_i}\}_{i=1}^d$.

4.1.4 Alignment. Using d independent models to learn and predict across d groups of inputs incurs an additional computational cost that scales linearly with d . To address this efficiency challenge, we employ the multi-input multi-output (MIMO) mechanism[15], utilizing a single forecasting model to independently learn from each of the d input groups and produce f outputs. This approach requires input alignment, which we achieve by projecting each input group through a separate linear layer to a shared dimension: $X_t^{P_i D} = \text{Linear}(X_t^{P_i}) \in \mathbb{R}^{N_i \times D}$, where D is the hidden dimension. As each group of patches $X_t^{P_i}$ will be input in parallel into the subsequent pipeline, and we abbreviate $X_t^{P_i}$ as X_t^P .

4.2 Transformer

We introduce a Transformer module to empower the model with long-term forecasting ability. With the Embedding matrices $\mathbf{W}^Q, \mathbf{W}^K, \mathbf{W}^V \in \mathbb{R}^{D \times D'}$, the input X_t^P is embedded into $\mathbf{Q}, \mathbf{K}, \mathbf{V} \in \mathbb{R}^{P \times D'}$, where $\mathbf{Q} = X_t^P \mathbf{W}^Q$, $\mathbf{K} = X_t^P \mathbf{W}^K$, $\mathbf{V} = X_t^P \mathbf{W}^V$, and D' is denoted as the hidden dimension for multi-head attention computation. After the Representer module and with positional encoding applied, the input is fed into an attention block with several attention layers. The multi-head self-attention (MHSA) mechanism allows the model to jointly attend to information from different representation subspaces at various positions:

$$\begin{aligned} \text{MHSA}(X_t^P) &= \text{Concat}(\text{head}_1, \dots, \text{head}_h) \mathbf{W}^O, \\ \text{where } \text{head}_i &= \text{Softmax}\left(\frac{\mathbf{Q}_i \mathbf{K}_i^T}{\sqrt{D'}}\right) \mathbf{V}_i, \\ \mathbf{Q}_i &= X_t^P \mathbf{W}_i^Q, \mathbf{K}_i = X_t^P \mathbf{W}_i^K, \mathbf{V}_i = X_t^P \mathbf{W}_i^V, \end{aligned} \quad (2)$$

where the projections are parameter matrices $\mathbf{W}_i^Q \in \mathbb{R}^{D \times D'}$, $\mathbf{W}_i^K \in \mathbb{R}^{D \times D'}$, $\mathbf{W}_i^V \in \mathbb{R}^{D \times D'}$, $\mathbf{W}^O \in \mathbb{R}^{hD' \times D}$ and D' denotes the hidden dimension for multi-head attention computation.

We construct an attention layer with MHSA, skip-connection, Batch Normalization [20], and a feed-forward network (FFN):

$$\mathbf{X}_A = \text{BatchNorm}(\mathbf{X}_t^P + \text{MHSA}(\mathbf{X}_t^P)), \quad (3)$$

$$\text{FFN}(\mathbf{X}_A) = \max(0, \mathbf{X}_A \mathbf{W}_1 + b_1) \mathbf{W}_2 + b_2, \quad (4)$$

$$\mathbf{X}_O = \text{BatchNorm}(\mathbf{X}_A + \text{FFN}(\mathbf{X}_A)), \quad (5)$$

where $\mathbf{W}_1 \in \mathbb{R}^{D \times D_{ff}}$, $\mathbf{W}_2 \in \mathbb{R}^{D_{ff} \times D}$, $b_1 \in \mathbb{R}^{D_{ff}}$, and $b_2 \in \mathbb{R}^D$. The output of an attention layer is fed into the next attention layer as input. Finally, We flatten output from the last attention block $\mathbf{X}_O \in \mathbb{R}^{P \times D}$ and map it to the final forecasting $\mathbf{Y}_t = f(\mathbf{X}) \in \mathbb{R}^H$ through a linear layer $\mathbf{Y}_t = \text{Linear}(\mathbf{X}_O)$.

4.3 Adapter

In the context of online training, the inherent noise and non-stationarity of time series data can lead to significant fluctuations in the gradient

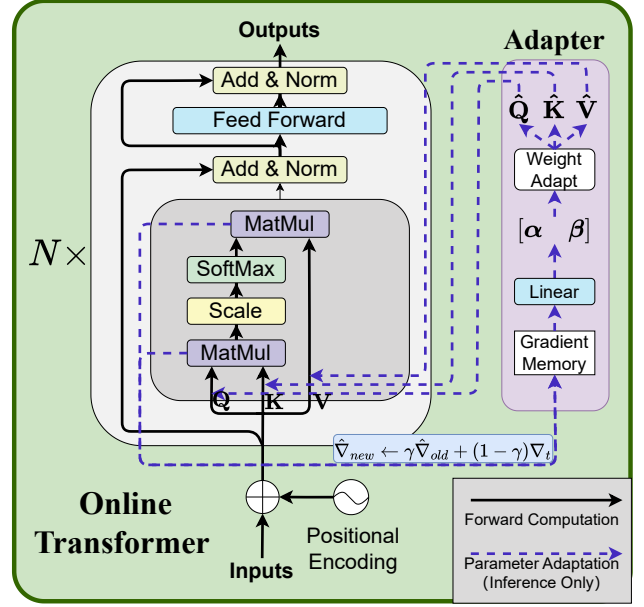


Figure 5: The structure of Online Transformer with Adapter. During the training phase, the Online Transformer's computation process aligns with that of the original Transformer Encoder, including self-attention layers, skip connections, batch normalization, and a feed-forward network (as shown by the solid black line). In the online inference phase, the Adapter adjusts the weights of the self-attention layer at the parameter level, enabling the model to dynamically adapt to data changes (as shown by the dashed blue line).

of a single sample, thereby introducing noise into the adaptation coefficients. To mitigate this issue, we draw inspiration from the ideas of FSNet [30] and employ the Exponential Moving Average (EMA) of the attention layers' gradient. This approach effectively smoothes the noise in online training, enabling efficient capture of the temporal information inherent in time series data:

$$\hat{\nabla}_{new} \leftarrow \gamma \hat{\nabla}_{old} + (1 - \gamma) \nabla_t, \quad (6)$$

where ∇_t denotes the gradient of the attention layer at time t and $\hat{\nabla}$ denotes the EMA gradient. The adaptor takes $\hat{\nabla}$ as input and maps it to the adaptation coefficients α, β . We adopt the element-wise transformation as the adaptation process thanks to its simplicity and promising results in continual learning [30, 39]. Particularly, the adaptation coefficients consist of two components: a weight adaptation coefficient α and a feature adaptation coefficient β . The adaptation process for an attention layer involves two steps: weight and feature transformations. First, we compute two adaptation coefficients by a linear layer fed with the flattened EMA gradient,

$$[\alpha, \beta] = \text{Linear}\left(\text{Flatten}(\hat{\nabla})\right). \quad (7)$$

Then, we apply weight adaptation to the parameter matrix $\mathbf{W}^Q, \mathbf{W}^K, \mathbf{W}^V$ and feature adaptation the hidden feature embeddings, respectively. Taking query embedding as an example:

$$\begin{aligned}\tilde{\mathbf{W}}^Q &= \alpha_l \odot \mathbf{W}^Q, \\ \mathbf{Q} &= \mathbf{X}_t^P \tilde{\mathbf{W}}_i^Q, \\ \tilde{\mathbf{Q}} &= \beta_l \odot \mathbf{Q}.\end{aligned}\quad (8)$$

Here, \mathbf{W}^Q is the query embedding weight matrix, $\tilde{\mathbf{W}}^Q$ denotes the adapted weight, \odot denotes the element-wise multiplication. Adapted query embedding $\tilde{\mathbf{Q}}$ will be used in Eq.(2) replacing \mathbf{Q} .

4.4 Ensembler

To generate robust predictions, it is necessary to integrate the forecasting results produced based on different levels of feature inputs. Accordingly, we have designed two ensemble module, Online Scaling and Follow The Perturbed Leader, of which the former achieves better performance while the other achieves better efficiency.

4.4.1 Online scaling: Choose the best expert with online convex optimization. Exponentiated Gradient Descent (EGD) [24] is a commonly used ensemble method. Specifically, the decision space Δ is a d -dimensional simplex, i.e. $\Delta = \{\mathbf{w}_t \mid w_{t,i} \geq 0 \text{ and } \|\mathbf{w}_t\|_1 = 1\}$, where t is the time step indicator and we omit the subscript t for simplicity when it's not confusing. Given the online data stream \mathbf{X} , its forecasting target \mathbf{Y} , and d forecasting experts with different parameters (in E^3Former there are d independent subnetworks with a part of shared parameters) $\mathbf{F} = [f_i(\mathbf{X})]_{i=1}^d$, the player's goal is to minimize the forecasting error as

$$\min_{\mathbf{w}} \left\| \sum_{i=1}^d w_i f_i(\mathbf{X}) - \mathbf{Y} \right\|^2 \quad \text{s.t.} \quad \mathbf{w} \in \Delta \quad (9)$$

According to EGD, choosing $\mathbf{w}_1 = [w_{1,i} = 1/d]_{i=1}^d$ as the center point of the simplex, the updating rule for each w_i will be

$$w_{t+1,i} = \frac{w_{t,i} \exp(-\eta \|f_i(\mathbf{X}) - \mathbf{Y}\|^2)}{Z_t} \quad (10)$$

where $Z_t = \sum_{i=1}^d w_{t,i} \exp(-\eta \|f_i(\mathbf{X}) - \mathbf{Y}\|^2)$ is the normalizer, and the algorithm can achieve the regret bound that is sublinear in T , the total time steps, signaling proficient long-term performance.

THEOREM 1. (Online convex optimization bound [12]) For $T > 2 \log(d)$, the EGD policy admits a vanishing regret

$$\text{Regret} = \sum_{t=1}^T \mathcal{L}(\mathbf{w}_t) - \inf_{\mathbf{u}} \sum_{t=1}^T \mathcal{L}(\mathbf{u}) = O(\sqrt{T}) \quad (11)$$

Nonetheless, it's a well-acknowledged issue that an exponentially weighted average forecaster tends to react sluggishly to significant shifts in data distribution. This response lag is often discussed in the context of online learning circles as the "slow switch phenomenon" [6]. Inspired by related algorithms [4, 35] developed to address this issue in online learning, we adopt the idea of finding an activation function that maps the original policy \mathbf{w}_t to a new one based on the recent loss of all experts.

Given the latest observed ground truth \mathbf{Y} , the set of corresponding d forecastings $\mathbf{F} = \{f_i(\mathbf{X})\}_{i=1}^d$ and the EGD weights $\mathbf{w} = \{w_i\}_{i=1}^d$, we employ an Online Scaling module to learn from the feedback and dynamically adjust the next forecasting, ensuring a

better fit with the actual series. We name this method $\text{E}^3\text{Former-OS}$. The Online Scaling module consists of an input embedding layer, a multi-head self-attention layer equipped with an Online Adaptor and an output linear layer. Input embedding layer stacks the forecastings and the ground truth together and maps the time dimension H to the hidden dimension D with a linear layer. After the input embedding layer, $\mathbf{F} \in \mathbb{R}^{d \times D}$ undergoes self-attention calculation, the process of which is described in Eq.(2) and Eq.(8). The output of the self-attention layer is flattened and fed into an linear layer to produce the scaling weights:

$$\mathbf{s} = \text{SoftMax}(\text{Linear}(\text{Flatten}(\text{MHSA}(\mathbf{F}))) + \mathbf{w}). \quad (12)$$

After undergoing EGD and Online Scaling, the model ultimately outputs an adapted result $\hat{\mathbf{f}} = \mathbf{s}^T \mathbf{F}$ that incorporates the optimized predictions from various stages of the process. We denote this model as $\text{E}^3\text{Former-OS}$, whose performance is evaluated in Section 5. Figure 7 presents its visualization results, demonstrating that after applying Online Scaling, the prediction outcomes are able to better align with the true values, particularly during periods where the model encounters concept drifts.

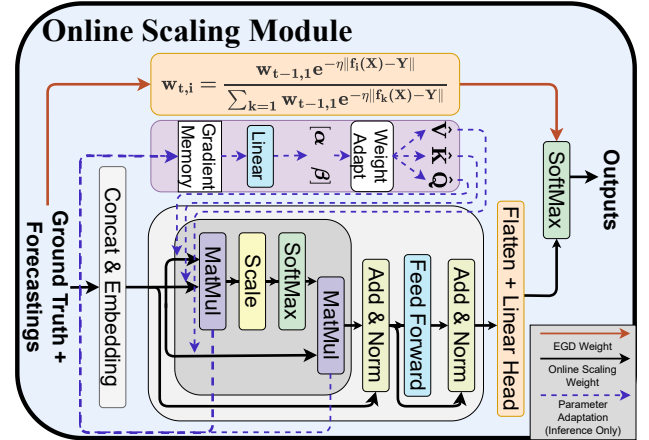


Figure 6: The structure of Online Scaling module.

4.4.2 Follow the perturbed leader: a more general method. EGD can achieve guaranteed results, but its effectiveness relies on the assumption that the prediction task can be framed as a convex optimization problem. However, in real-world tasks, it is often difficult to make such an assumption about the environment. Therefore, we also introduce another classical online method, Follow The Perturbed Leader (FTPL) [22], into our algorithm, which we name $\text{E}^3\text{Former-FTPL}$. FTPL has been proven to yield good performance in both convex and non-convex optimization settings [34]. Furthermore, since it is essentially a non-parametric approach, it boasts efficiency advantages over EGD, potentially making it a more versatile and generalizable choice. Specifically, the decision space Π encompasses a set of feasible actions or strategies π_t (which expert, or result from a subnetwork, to choose), i.e., $\Pi = \{\pi_t \mid \pi_{t,i} \in [0, 1] \text{ and } \|\pi_t\|_1 = 1\}$. In an online setting, given \mathbf{x} and \mathbf{y} , the algorithm also seeks to minimize the cumulative loss over time.

The core principle of FTPL involves introducing a random perturbation to the decision-making process, thereby allowing for

exploration within the decision space. This is formalized as follows:

$$\pi_{t+1} = \arg \min_{\pi \in \Pi} \left\{ \sum_{\tau=1}^t \|f_{\pi}(\mathbf{X}_{\tau}) - \mathbf{Y}_{\tau}\|^2 + \sigma(\pi) \right\} \quad (13)$$

where $\sigma(\pi)$ represents the perturbation added to the cumulative loss, often derived from a predefined noise distribution (in this work we use Uniform distribution). The updating mechanism, according to FTPL, is predicated on combining historical performance data with present stochasticity introduced through $\sigma(\pi)$. This strategic addition of randomness is aimed at mitigating the algorithm’s propensity for short-term myopia, thus enhancing its exploratory capabilities and overall adaptability to evolving contexts. The complete procedure of FTPL is shown in Alg. 1.

Algorithm 1: Follow The Perturbed Leader (FTPL)

Input: Pool of different sub-networks $\mathcal{F} = \{f_i\}_{i=1}^d$, Time stamp t , Perturbation distribution \mathbb{D}_{per} , Loss function ℓ , Repeat times m .

Output: Target model f .

```

1 for  $j = 1, \dots, m$  do
2   foreach base model  $f^i \in \mathcal{F}$  do
3     Sample the perturbation  $\sigma(i) \sim \mathbb{D}_{per}$ ;
4   Get the decision  $\pi_{t+1,j}$  according to the Eqn. (13);
5 Sample  $f$  from the empirical distribution over
    $\{\pi_{t+1,1}, \pi_{t+1,2}, \dots, \pi_{t+1,m}\}$  as the target model;
```

THEOREM 2. [7] *Given decision space Π , the expectation of regret for Follow the Perturbed Leader has a sublinear bound:*

$$\mathbb{E}[\text{Regret}] = \mathbb{E}\left[\sum_{t=1}^T \mathcal{L}(\pi_t) - \inf_{\mathbf{u}} \sum_{t=1}^T \mathcal{L}(\mathbf{u})\right] = O(\sqrt{T}) \quad (14)$$

The theoretical underpinning of FTPL establishes that, under appropriate conditions concerning the perturbation type and algorithmic parameters, it can achieve a vanishing regret that is sublinear in T , the total number of time steps, signaling proficient long-term performance.

We denote this model as E³Former-FTPL. In the majority of comparisons show in Section 5, E³Former-FTPL marginally underperforms relative to E³Former-OS. Nonetheless, it offers the benefits of reduced parameter count and expedited inference speeds, contributing to greater throughput as shown in Figure 8 and facilitating flexible deployment in environments limited by resources.

5 EXPERIMENTS

5.1 Experimental setting

5.1.1 Datasets. To comprehensively evaluate the performance and generalization capability of our model, we conduct extensive experiments on twelve datasets, including six workload datasets gathered from the Bytedance Cloud platform and six public time series datasets, as shown in Table 3. Based on the Bytedance Cloud platform, we conduct a 16-day experiment in the private cloud platform and 49-day experiment in the public cloud platform (with workload data at minute-level granularity, predicting once every hour):

Table 3: Summary of the datasets

Category	Dataset	Domain	Variates	Samples	Frequency
Public	ETTh1	Industry	7	17420	1 hour
	ETTh2	Industry	7	17420	1 hour
	ETTm1	Industry	7	69680	15 min
	ETTm2	Industry	7	69680	15 min
	Electricity	Energy	321	26304	1 hour
	Weather	Environment	21	52696	1 hour
Private	FaaS_Small	Private Cloud	7	23041	1 min
	FaaS_Medium	Private Cloud	93	23041	1 min
	FaaS_Large	Private Cloud	226	23041	1 min
	IaaS_Small	Public Cloud	7	69764	1 min
	IaaS_Medium	Public Cloud	58	69764	1 min
	IaaS_Large	Public Cloud	93	69764	1 min

- The **FaaS** dataset, including FaaS_Small, FaaS_Medium, and FaaS_Large, comprises query-per-second data gathered from the Function-as-a-Service (FaaS) service.
- The **IaaS** dataset, including IaaS_Small, IaaS_Medium, IaaS_Large, comprises CPU usage data gathered from the Infrastructure-as-a-Service (IaaS) service.

Additionally, to assess the generalizability of the proposed model, we carry out extra experiments on public time series datasets:

- The **ETT**³ dataset, including ETTh1, ETTh2, ETTm1 and ETTm2, comprises load and oil temperature data from two power transformers at different stations.
- The **Electricity**⁴ dataset includes electricity consumption data, measured in kilowatt-hours (kWh), from 321 clients, spanning from 2012 to 2014.
- The **Weather**⁵ dataset consists of meteorological indicators, sampled every 10 minutes, covering the entire year of 2020.

5.1.2 Baselines. We selected four categories of time series forecasting models as baselines:

- (1) Extensively applied traditional statistical models such as ETS [19], Seasonal ARIMA [36], and STL [9].
- (2) Representative deep neural networks for time series forecasting models (tested with retraining setting), such as MLP-based DLinear [40], CNN-based TimesNet [38], Transformer-based iTransformer [26] and PatchTST [29].
- (3) LLM-based time series forecasting models designed for few-shot and zero-shot forecasting, GPT4TS [43] (tested in two manners: offline forecasting following the original setting and online forecasting with retraining).
- (4) Neural networks for online prediction, such as FSNet [30], OneNet [35], and Time-FSNet, a variant of FSNet, which modifies the dimensionality of convolutional computations.

5.1.3 Implemental Details. For FaaS and IaaS datasets, we leverage a week’s archive of offline data for training the models, which are deployed in an online configuration. The models forecast workload data at fixed intervals, for instance, every 60 minutes, without any overlap between successive predictions to conserve computational

³<https://github.com/zhouhaoyi/ETDataset>

⁴<https://archive.ics.uci.edu/ml/datasets/ElectricityLoadDiagrams20112014>

⁵<https://www.bgc-jena.mpg.de/wetter/>

Table 4: Results for the forecasting task on the cloud system workload datasets. The input sequence length is set to 1440. All the results are averaged from 4 different forecasting horizons {1, 10, 30, 60}.

Datasets Metric	FaaS_Small			FaaS_Medium			FaaS_Large			IaaS_Small			IaaS_Medium			IaaS_Large		
	MSE	MAE	WMAPE	MSE	MAE	WMAPE	MSE	MAE	WMAPE	MSE	MAE	WMAPE	MSE	MAE	WMAPE	MSE	MAE	WMAPE
STL[9]	1.303	0.803	6.339	1.453	0.860	6.885	3.168	1.105	21.320	1.750	1.006	1.317	1.715	1.034	1.225	1.742	1.032	1.131
SARIMA[36]	1.150	0.728	4.102	1.288	0.790	6.511	3.025	1.059	20.685	1.237	0.836	1.065	1.290	0.891	1.034	1.329	0.888	0.958
ETS[19]	1.222	0.749	6.113	1.358	0.811	6.662	3.128	1.073	20.915	1.318	0.858	1.097	1.305	0.896	1.038	1.337	0.887	0.952
DLinear[40]	3.401	1.003	7.225	3.368	1.033	10.602	0.267	0.288	3.629	0.748	0.615	0.737	0.902	0.753	0.827	0.970	0.773	0.816
TimesNet[38]	0.596	0.542	3.846	0.525	0.499	3.423	0.922	0.571	10.015	0.828	0.665	0.829	0.858	0.769	0.862	0.901	0.794	0.828
PatchTST[29]	0.327	0.370	3.787	0.290	0.334	1.999	0.479	0.391	6.728	0.689	0.582	0.701	0.804	0.711	0.787	0.830	0.723	0.756
iTransformer[26]	0.298	0.352	2.345	0.287	0.331	1.977	0.340	0.318	5.171	0.840	0.692	0.838	0.830	0.753	0.831	0.868	0.759	0.775
GPT4TS[43]	0.262	0.333	2.145	0.235	0.296	1.715	0.245	0.267	4.042	0.666	0.565	0.679	0.755	0.675	0.743	0.749	0.701	0.718
Online-GPT4TS	0.253	0.329	2.096	0.244	0.314	1.927	0.286	0.318	5.343	0.645	0.577	0.717	0.760	0.700	0.767	0.765	0.719	0.733
FSNet[30]	0.271	0.321	1.930	0.265	0.325	2.281	0.266	0.329	2.425	0.672	0.588	0.696	0.797	0.721	0.783	0.841	0.743	0.776
Time-FSNet[30]	0.249	0.320	2.054	0.228	0.298	1.827	0.237	0.306	1.801	0.734	0.629	0.754	0.790	0.732	0.807	0.833	0.746	0.775
OneNet[35]	0.228	0.294	1.709	0.229	0.293	1.781	0.229	0.293	1.781	0.674	0.599	0.705	0.777	0.718	0.785	0.761	0.709	0.725
E³Former-FTPL	0.208	0.270	1.477	0.214	0.274	1.381	0.214	0.274	1.385	0.646	0.565	0.669	0.741	0.692	0.751	0.753	0.691	0.707
E³Former-OS	0.203	0.263	1.419	0.208	0.267	1.281	0.217	0.277	1.445	0.634	0.563	0.665	0.733	0.689	0.746	0.734	0.682	0.695

WMAPE indicates that we multiply the WMAPE by 100 on FaaS data to better display and compare the results.

resources. Over the course of our research, the model performs online predictions for a duration of one week on FaaS and six weeks on IaaS. We follow the optimization details in Informer [42] by optimizing the ℓ_2 (MSE) loss with the AdamW optimizer [27]. For all benchmarks, we set the look-back window length to be 1440 (is the maximum reasonable query length that the cloud computing system we are using can handle online) and vary the forecast horizon as $H \in \{1, 10, 30, 60\}$. During the training phase, the batch size for all models is set to 32, except for GPT4TS, which is set to 8 to avoid GPU memory overflow. The hyperparameters for all models are configured based on their official implementations or implementations found in other research papers. Specifically, for the proposed model, we chose a group of patch sizes {16, 32, 64, 128} and During the parameter analysis, this selection will be expanded to include {16, 32, 64, 128, 256, 512}.

All experiments are repeated three times, implemented in PyTorch and conducted on NVIDIA Tesla V100 32GB GPUs. All the baselines are implemented based on configurations of the original paper or official code. For the metrics, we adopt the mean square error (MSE), mean absolute error (MAE), and mean absolute percentage errors (WMAPE) for long-term forecasting and imputations, where MSE and MAE are calculated after the data has been standard normalized, whereas WMAPE is calculated after normalization and denormalization. These metrics can be calculated as follows:

$$MSE = \frac{1}{M} \sum_{j=1}^M \left\| \hat{x}_{t+1:t+H}^j - x_{t+1:t+H}^j \right\|,$$

$$MAE = \frac{1}{M} \sum_{j=1}^M \left| \hat{x}_{t+1:t+H}^j - x_{t+1:t+H}^j \right|,$$

$$WMAPE = \frac{\sum_{j=1}^M \left| \hat{x}_{t+1:t+H}^j - x_{t+1:t+H}^j \right|}{\sum_{k=1}^M x_{t+1:t+H}^k}.$$

5.2 Online Forecasting Results

In this setting, the data used for training and online forecasting is from the same time series. Table 4 and Table 5 present the cumulative performance of different baselines in terms of mean-squared errors (MSE), mean-absolute errors (MAE), and weighted mean absolute percentage errors (WMAPE), where MSE and MAE are calculated after the data has been standard normalized, whereas WMAPE is calculated after normalization and denormalization. The workload data from FaaS demonstrates significant periodicity, typically leading to comparatively lower prediction errors in models. Models operating online, like OneNet, generally surpass the performance of offline models that necessitate retraining, exemplified by iTransformer. This performance discrepancy is attributed to the clear data drift characteristic of FaaS data. Despite the data being minutely granular, it also captures broader cycles on daily, weekly, and monthly scales. Offline models, despite undergoing retraining, face difficulties in accurately adapting to these evolving features. LLM-based GPT4TS shows good performance, but its parameter volume far exceeds that of other models. Our proposed E³Former-OS and E³Former-FTPL have demonstrated superior performance compared to the baselines. Specifically, E³Former-OS reduces MSE by 13.9%, MAE by 11.7%, and WMAPE by 19.3% on average across seven datasets compared to the best baseline, OneNet (E³Former-FTPL exceeded it by 9.2%/8.5%/13.3%).

5.3 Online Transfer Forecasting Results

Online transfer forecasting involves training a model within one dataset and then applying it to another dataset, necessitating a substantially higher adaptability to unknown data. In the transfer experiments, we evaluate the model’s ability from multiple aspects:

- (1) Transfer between datasets with the same resolution within the same domain (FaaS→FaaS and IaaS→IaaS).
- (2) Transfer between datasets with the same resolution across different domains (FaaS→IaaS and IaaS→FaaS).

Table 5: Results for the forecasting task on the other public datasets. The input sequence length is set to 1440. All the results are averaged from 4 different forecasting horizons {1, 10, 30, 60}.

Datasets Metric	ETTh1			ETTh2			ETTh1			ETTh2			ECL			Weather		
	MSE	MAE	WMAPE	MSE	MAE	WMAPE	MSE	MAE	WMAPE	MSE	MAE	WMAPE	MSE	MAE	WMAPE	MSE	MAE	WMAPE
STL[9]	1.757	0.992	1.176	1.702	0.933	0.562	3.152	1.283	0.756	3.938	1.368	0.323	1.484	0.821	0.335	6.555	1.697	0.576
SARIMA[36]	1.890	0.917	1.021	1.689	0.905	0.541	2.882	1.137	0.671	3.688	1.239	0.292	1.337	0.776	0.316	5.594	1.441	0.475
ETS[19]	2.563	1.062	1.166	1.654	0.897	0.537	2.899	1.145	0.675	3.753	1.255	0.294	1.511	0.807	0.328	5.820	1.468	0.485
DLinear[40]	0.282	0.359	0.376	0.162	0.259	0.149	0.346	0.429	0.219	0.355	0.391	0.073	0.182	0.254	0.090	0.642	0.374	0.107
TimesNet[38]	0.464	0.482	0.521	0.307	0.386	0.225	0.671	0.561	0.301	0.621	0.558	0.119	0.352	0.348	0.112	1.457	0.754	0.165
PatchTST[29]	0.335	0.401	0.419	0.160	0.268	0.157	0.398	0.414	0.214	0.366	0.400	0.077	0.201	0.257	0.083	0.815	0.458	0.124
iTransformer[26]	0.294	0.371	0.401	0.180	0.281	0.163	0.503	0.485	0.263	0.520	0.510	0.106	0.202	0.258	0.088	1.057	0.605	0.154
GPT4TS[43]	0.311	0.383	0.419	0.160	0.264	0.153	0.319	0.385	0.205	0.351	0.410	0.084	-	-	-	0.688	0.419	0.109
Online-GPT4TS	0.382	0.430	0.482	0.174	0.277	0.159	0.405	0.451	0.248	0.434	0.463	0.095	-	-	-	1.195	0.658	0.183
FSNet[30]	0.354	0.416	0.418	0.213	0.311	0.178	0.651	0.534	0.290	1.825	0.903	0.205	0.310	0.349	0.121	0.952	0.598	0.220
Time-FSNet[30]	0.315	0.389	0.418	0.267	0.356	0.201	0.443	0.479	0.284	0.431	0.460	0.096	0.198	0.280	0.096	0.959	0.590	0.184
OneNet[35]	0.297	0.374	0.387	0.188	0.296	0.166	0.395	0.432	0.241	0.417	0.444	0.090	0.189	0.272	0.095	0.694	0.430	0.135
E³Former-FTPL	0.285	0.362	0.373	0.155	0.258	0.148	0.319	0.384	0.195	0.333	0.374	0.071	0.180	0.246	0.087	0.602	0.356	0.099
E³Former-OS	0.275	0.352	0.365	0.150	0.252	0.143	0.282	0.342	0.174	0.328	0.371	0.071	0.171	0.242	0.083	0.626	0.368	0.103

- CUDA out of memory.

Table 6: Results for the transfer forecasting task. All models are pre-trained on the source dataset and tested on the target dataset. For the same domain, such as FaaS, we randomly collect 7 different clusters from the system to construct the source and target. All the results are averaged from 4 different forecasting horizons {1, 10, 30, 60}.

Datasets Metric	FaaS→FaaS			IaaS→IaaS			FaaS→IaaS			IaaS→FaaS			ETTh1→ETTh1			ETTh2→ETTh2			FaaS→Weather		
	MSE	MAE	WMAPE	MSE	MAE	WMAPE	MSE	MAE	WMAPE	MSE	MAE	WMAPE	MSE	MAE	WMAPE	MSE	MAE	WMAPE	MSE	MAE	WMAPE
STL[9]	4.851	1.228	0.196	1.717	1.024	1.007	1.750	1.006	1.317	1.303	0.803	0.063	3.152	1.283	0.756	1.423	0.773	0.351	6.555	1.697	0.576
SARIMA[36]	4.726	1.193	0.194	1.353	0.889	0.865	1.237	0.836	1.065	1.150	0.728	0.059	2.882	1.137	0.671	1.297	0.710	0.323	5.594	1.441	0.475
ETS[19]	4.696	1.187	0.191	1.424	0.923	0.900	1.339	0.886	1.131	1.261	0.761	0.061	2.899	1.145	0.675	1.290	0.712	0.324	5.542	1.441	0.476
DLinear[40]	12.478	1.785	0.389	1.339	0.947	0.966	1.363	0.900	1.230	0.661	0.530	0.037	0.417	0.442	0.226	0.275	0.303	0.119	2.514	0.897	0.329
TimesNet[38]	2.233	0.938	0.161	1.451	0.987	0.988	1.408	0.926	1.151	0.901	0.695	0.057	0.769	0.644	0.347	0.752	0.528	0.229	5.053	1.521	0.470
PatchTST[29]	1.027	0.571	0.087	1.165	0.888	0.876	0.999	0.785	0.930	3.104	0.845	0.050	0.550	0.498	0.256	0.320	0.341	0.138	2.135	0.892	0.302
iTransformer[26]	0.714	0.431	0.061	1.133	0.871	0.848	1.306	0.887	1.079	0.617	0.567	0.041	0.718	0.610	0.335	0.333	0.355	0.148	1.698	0.736	0.215
GPT4TS[43]	0.592	0.380	0.049	1.003	0.856	0.834	1.159	0.810	0.986	0.870	0.657	0.047	0.461	0.463	0.249	0.305	0.329	0.136	1.411	0.681	0.208
Online-GPT4TS	0.718	0.508	0.086	0.993	0.842	0.827	1.090	0.814	0.998	0.623	0.482	0.033	0.448	0.475	0.256	0.338	0.346	0.143	1.202	0.670	0.188
FSNet[30]	1.227	0.566	0.081	1.309	0.940	0.973	1.398	0.955	1.221	1.517	0.913	0.077	0.603	0.553	0.318	0.670	0.544	0.228	1.539	0.810	0.286
Time-FSNet	0.949	0.586	0.100	1.107	0.876	0.846	1.016	0.811	0.955	0.594	0.545	0.041	0.556	0.312	0.533	0.303	0.356	0.149	0.966	0.623	0.236
OneNet[35]	0.511	0.441	0.077	1.082	0.868	0.871	0.965	0.771	0.916	0.627	0.559	0.039	0.424	0.456	0.252	0.323	0.359	0.152	1.052	0.609	0.185
E³Former-FTPL	0.499	0.345	0.045	1.086	0.864	0.860	0.970	0.783	0.924	0.623	0.501	0.034	0.389	0.419	0.222	0.275	0.302	0.120	1.086	0.610	0.179
E³Former-OS	0.396	0.330	0.042	0.982	0.829	0.823	0.909	0.749	0.885	0.531	0.469	0.031	0.356	0.405	0.215	0.264	0.296	0.117	1.029	0.581	0.159

- (3) Transfer between datasets with the different resolutions within the same domain (ETTh1→ETTh1 and ETTh1→ETTh2).
- (4) Transfer between datasets with the different resolutions across different domains (FaaS→Weather).

The aggregate outcomes are detailed in Table 6. Predominantly, online models outshine retrained offline models in transfer tasks, illustrating that online predictions possess significant advantages over offline predictions in scenarios characterized by cold starts and the introduction of new data. Notably, the E³Former-OS’s performance significantly surpasses that of established baselines, achieving a reduction in MSE by 15.3%, MAE by 14.1%, and WMAPE by 26.3% on average, when compared to the leading baseline, OneNet, across a suite of six transfer tasks (with E³Former-FTPL also outperforming it, albeit by smaller margins of 3.1%, 7.9%, and 13.1%).

5.4 Ablation Study and Further Discussion

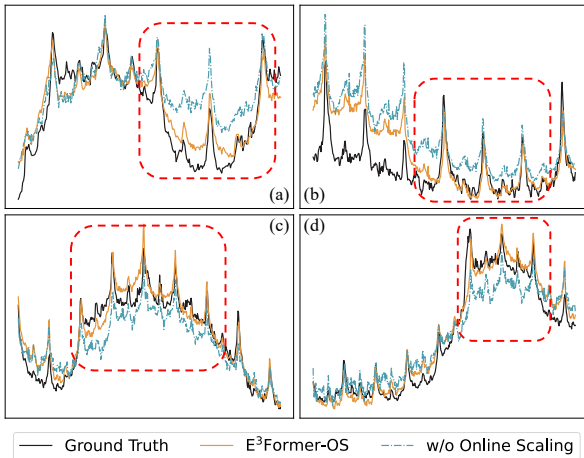
5.4.1 Ablation study. Our analysis delves into the contribution of each component within the model. Initially, we investigate the advantages of employing the MIMO mechanism by utilizing a single patch size, without which E³Former consists of only one subnetwork, no longer forming an ensemble model. Subsequently, we omit the online adaptor in the online Transformer backbone, reducing it to a basic transformer block. Specifically, the removal of MIMO and the online adaptor from our model results in its simplification to a PatchTST.

These pertinent findings are recorded in Table 7. A key observation is the critical nature of both components, where the absence of either leads to a substantial decline in performance. For instance, excluding MIMO from E³Former-OS results in an

Table 7: Results for the ablation study. We compare extensive competitive models under different prediction lengths. The input sequence length is set to 1440. Avg is averaged from all four prediction lengths.

Models	E ³ Former-OS			w/o MIMO			w/o Online Adaptor			E ³ Former-FTPL			w/o MIMO			w/o Online Adaptor			Online PatchTST			
Metric	MSE	MAE	WMAPE	MSE	MAE	WMAPE	MSE	MAE	WMAPE	MSE	MAE	WMAPE	MSE	MAE	WMAPE	MSE	MAE	WMAPE	MSE	MAE	WMAPE	
FaaS	1	0.087	0.177	0.707	0.087	0.198	0.676	0.094	0.188	0.765	0.089	0.177	0.703	0.088	0.194	0.678	0.092	0.180	0.698	0.091	0.169	0.684
	10	0.174	0.260	1.240	0.198	0.280	1.234	0.184	0.274	1.378	0.184	0.271	1.365	0.194	0.276	1.206	0.188	0.276	1.487	0.208	0.292	1.357
	30	0.217	0.302	1.487	0.248	0.336	1.665	0.223	0.310	1.632	0.218	0.304	1.526	0.254	0.340	1.656	0.230	0.319	1.730	0.299	0.363	1.928
	60	0.354	0.328	1.688	0.368	0.340	1.788	0.362	0.338	1.829	0.366	0.343	1.931	0.372	0.348	1.821	0.369	0.344	1.961	0.430	0.398	2.166
	Avg	0.208	0.267	1.281	0.225	0.289	1.341	0.216	0.278	1.401	0.214	0.274	1.381	0.227	0.290	1.338	0.220	0.280	1.469	0.257	0.306	1.534
IaaS	1	0.421	0.392	0.474	0.453	0.402	0.488	0.481	0.420	0.504	0.423	0.388	0.471	0.457	0.402	0.483	0.464	0.411	0.485	0.476	0.407	0.494
	10	0.552	0.520	0.622	0.587	0.533	0.664	0.584	0.525	0.629	0.580	0.524	0.628	0.587	0.535	0.666	0.596	0.533	0.633	0.611	0.542	0.665
	30	0.735	0.632	0.734	0.753	0.641	0.761	0.756	0.639	0.745	0.742	0.641	0.754	0.754	0.643	0.766	0.765	0.653	0.762	0.792	0.652	0.777
	60	0.828	0.708	0.829	0.887	0.747	0.920	0.856	0.725	0.848	0.839	0.706	0.823	0.885	0.747	0.915	0.891	0.761	0.896	0.876	0.726	0.867
	Avg	0.634	0.563	0.665	0.670	0.581	0.708	0.669	0.577	0.682	0.646	0.565	0.669	0.671	0.582	0.707	0.679	0.590	0.694	0.689	0.582	0.701
FaaS→FaaS	1	0.161	0.185	0.028	0.184	0.183	0.027	0.243	0.208	0.034	0.235	0.185	0.027	0.182	0.181	0.026	0.217	0.218	0.030	0.374	0.208	0.028
	10	0.291	0.313	0.042	0.472	0.407	0.068	0.461	0.378	0.046	0.456	0.335	0.043	0.490	0.424	0.070	0.521	0.414	0.056	0.657	0.526	0.058
	30	0.459	0.371	0.043	0.500	0.404	0.068	0.813	0.580	0.070	0.482	0.419	0.051	0.499	0.401	0.061	0.778	0.570	0.071	1.157	0.705	0.078
	60	0.672	0.452	0.055	0.709	0.451	0.064	1.109	0.606	0.066	0.824	0.439	0.057	0.704	0.451	0.064	1.180	0.673	0.081	1.276	0.715	0.084
	Avg	0.396	0.330	0.042	0.466	0.361	0.055	0.657	0.443	0.054	0.499	0.345	0.045	0.469	0.364	0.055	0.674	0.469	0.060	0.866	0.539	0.062
ETTh1→ETTh1	1	0.088	0.199	0.096	0.089	0.199	0.096	0.091	0.202	0.099	0.085	0.200	0.099	0.086	0.199	0.096	0.094	0.205	0.101	0.092	0.206	0.101
	10	0.273	0.366	0.189	0.366	0.415	0.208	0.355	0.407	0.205	0.354	0.403	0.198	0.372	0.420	0.209	0.364	0.409	0.206	0.431	0.453	0.225
	30	0.466	0.495	0.269	0.623	0.574	0.320	0.659	0.583	0.303	0.477	0.501	0.272	0.611	0.567	0.315	0.690	0.602	0.319	0.770	0.633	0.328
	60	0.596	0.559	0.304	0.746	0.624	0.342	0.923	0.697	0.367	0.640	0.570	0.317	0.726	0.620	0.340	0.910	0.696	0.369	1.018	0.732	0.376
	Avg	0.356	0.405	0.215	0.456	0.453	0.241	0.507	0.472	0.244	0.389	0.419	0.222	0.449	0.452	0.240	0.515	0.478	0.249	0.578	0.506	0.258

increase in MSE/MAE/WMAPE by 15.0%, 8.2%, and 13.4%, respectively, and the removal of the online adaptor sees these metrics escalate by 29.4%, 14.3%, and 13.5%, respectively. These trends are consistent for E³Former-FTPL. Notably, in transfer tasks, the importance of the online adaptor is magnified, with its exclusion causing MSE/MAE/WMAPE in E³Former-OS to soar by 54.2%, 25.4%, and 21.0%, respectively, underscoring the adaptor's role in tackling cold starts and domain shifts.

**Figure 7: Visualizing E³Former-OS's forecasting.**

5.4.2 Efficiency analysis. We evaluated the parameter count and the average throughput of various online models to measure their efficiency, with results illustrated in Fig. 8. Each model was tested using Nvidia Tesla V100 32GB GPUs. Among these, E³Former-OS and E³Former-FTPL stand out for delivering not only precise forecasts but also the highest throughput levels. OneNet's inference time was notably longer than that of other models. This increased time is attributed to OneNet's ensemble setup, which involves the sequential application of two FSNet models. E³Former-FTPL showed a significant reduction in inference time—39.6% less than that of OneNet. Additionally, the parameter count of E³Former is significantly reduced, for example, E³Former-FTPL constituting merely 16.7% of OneNet's total. This reduction enables it to attain a throughput that astonishingly exceeds OneNet's by over **800%**.

5.4.3 Forecasting results visualization. Some examples of forecasting results for E³Former-OS on FaaS are visualized in Fig. 7. The dashed cyan line represents the prediction results of E³Former-OS without Online Scaling. We can intuitively observe that after applying Online Scaling, the prediction results better fit the real sequence, especially during the process of trend drifts in the sequence. Additionally, the illustration in Fig. 9 showcasing the dynamic changes in the weights of different base models within E³Former-OS during the inference process, underscores the model's ability to swiftly adapt to shifts in sequential patterns. This rapid adjustment of weights is a crucial aspect that addresses the issues "slow switch phenomenon" [6], where static or slow-adapting models often struggled to maintain high predictive accuracy in the face of evolving data distributions.

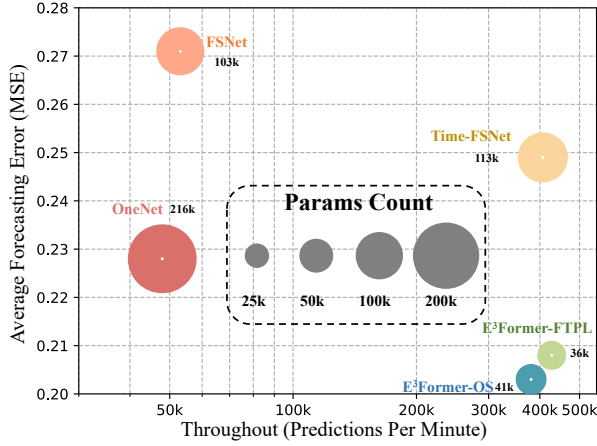


Figure 8: Model performance and throughput comparison.

5.4.4 Effects of number of subnetworks. Fig. 10 shows the performance of E³Former-OS as the patch size group varies. E³Former with a patch size group {16} is equivalent to a PatchTST since there is only one subnetwork. As the grows of the number of subnetworks, we can see that the errors of E³Former-OS slowly decline as they utilize more of the network capacity. The number of subnetworks contained in patch sizes {16, 32, 64, 128} and {16, 32, 64, 128, 256, 512} differs by 50%, yet their performance is comparable, with the former even outperforming the latter in some cases (FaaS→IaaS). This could be attributed to the fact that the network capacity is nearing its limit, whereafter the improvement in model performance due to an increase in the number of subnetworks exhibits a diminishing marginal effect. Therefore, considering the balance between efficiency and effectiveness, we generally utilized models with 4 subnetworks (patch sizes {16, 32, 64, 128}) in the experiments.

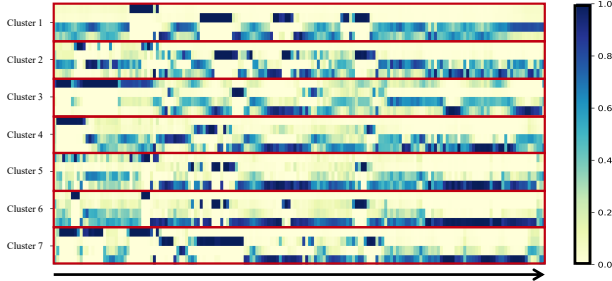


Figure 9: The variation of weights among different base models during the online inference process of E³Former-OS.

5.5 Kubernetes Horizontal Pod Autoscaling

To explore the value of workload forecasting models in real-world tasks, the best approach would be to deploy them in online auto-scaling systems. However, online environments are often highly complex, comprising numerous components and rules, and the complexity makes it infeasible to isolate and measure the performance of forecasting models using controlled experiments. Moreover, online services typically have very low tolerance for high latency,

making it difficult to conduct long-term online tests at the risk of degrading service quality. These factors render it impractical to rely on online testing to assess the value of forecasting models.

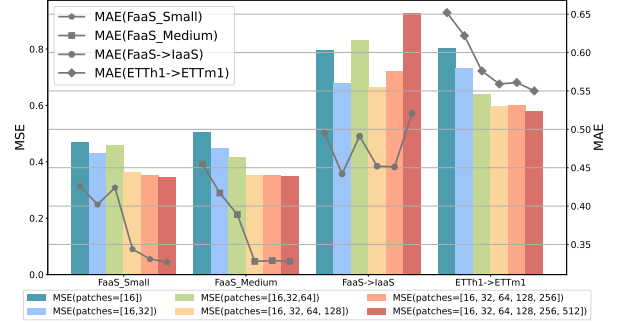


Figure 10: The performance of E³Former-OS as the number of subnetworks varies from 1 to 6.

To evaluate the performance of E³Former in a real-world production setting, we construct a controlled Kubernetes system and perform a comparative analysis against other forecasting models within the framework of Kubernetes Horizontal Pod Autoscaling (HPA). Prior research, including AHPA[44], has highlighted the benefits of predictive HPA over traditional reactive approaches, attributing these advantages to the mitigation of performance degradation due to pod initialization delays. In our experiment, as shown in Figure 11, we deploy a test service on a Kubernetes cluster, subjecting it to a workload pattern derived from historical QPS data sourced from a FaaS cluster. We conduct offline model training based on the data collected by the system over the past two weeks. At the commencement of each scaling interval (defaulting to 1 minute), scaling decisions are executed based on the predicted workload for that interval. At regular intervals (defaulting to 10 minutes), the system review forecasting errors based on real-time metrics and performs online model updates.

We integrate each forecasting model into the Kubernetes HPA system and monitor the latency and resource consumption of the pods over a two-week period. For the Ideal strategy, these decisions are informed by actual future workload data. Our analysis encompasses comparisons between HPAs leveraging various forecasting

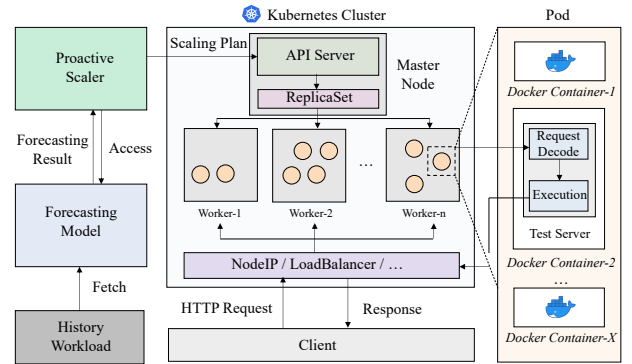


Figure 11: kubernetes Horizontal Pod Auto-Scaler System.

models, the Naïve HPA included with Kubernetes, and the Ideal HPA with foresight into future workloads (AHPA is excluded as it is not open-sourced), with results presented in Table 8. It is important to recognize that assessing HPA based solely on latency or resource utilization is not appropriate. If we were to allocate nearly unlimited physical resources to the system, latency would be minimal (or, conversely, if we allocated only one Pod, resource usage would be minimal, though latency would be uncontrollable). However, this is not aligned with best practices for cloud systems.

Table 8: Results of predictive Kubernetes Horizontal Pod Autoscaling. *Ave* stands for Average, *99.9-Lat*, *99-Lat* and *90-Lat* represents the 99.9, 99 and 90 percentile latency.

Models	Ave-Lat(s)	Max-Lat(s)	99.9-Lat(s)	99-Lat(s)	90-Lat(s)	AvePod	MaxPod
iTransformer	0.264	63.156	3.277	1.224	0.422	15.610	19
FSNet	0.236	7.347	2.321	1.039	0.405	14.942	29
OneNet	0.267	52.906	3.085	1.217	0.430	14.949	22
Naïve HPA	0.231	91.022	8.275	0.689	0.343	16.574	34
Ideal	0.219	9.419	2.087	0.739	0.371	14.608	24
E ³ Former-FTPL	0.223	7.734	2.072	0.767	0.380	15.071	22
E ³ Former-OS	0.218	7.535	1.953	0.731	0.368	15.368	21

Our research indicates that the E³Former effectively forecasts future workloads, thereby enhancing Quality of Service (QoS). This improvement is evidenced by a roughly 30% reduction in the 99th percentile (p99) latency and efficient resource utilization, as reflected by the average number of pods. Comparatively, E³Former achieves lower latency and uses fewer pods than other forecasting models. For example, E³Former-FTPL demonstrates a 16.5% improvement in average latency over OneNet, without a significant increase in pod usage. We note that HPAs guided by other forecasting models have also performed well in certain metrics. For instance, the iTransformer-based HPA strategy has the lowest maximum pod occupation, though with the highest average latency. Conversely, the FSNet-based HPA strategy has the lowest maximum latency (Max-Lat), but with the highest number of maximum pod occupations. In contrast, E³Former strikes the best balance between latency and resource utilization. Moreover, HPAs based on E³Former outperform the Naïve HPA in both average and peak latency metrics while using fewer pods. Notably, E³Former-OS reduces maximum latency by 91.7% compared to the Naïve HPA. E³Former offers a similar QoS to the ideal HPA, albeit with a slightly higher average number of pods.

Current predictive auto-scaling systems are bottlenecked by their reliance on historical data; for example, for predictive auto-scaling, AWS ECS⁶ requires at least 24 hours (two weeks being ideal) of historical data (3, 7, 7 days for Google Cloud⁷, Azura⁸, and Alibaba Cloud⁹, respectively), which restricts their deployment with limited historical data (so-called *cold-start* tasks). To evaluate our model’s performance in cold-start scenarios, we conducted Kubernetes HPA experiments where the forecasting models were pretrained offline on data from other FaaS clusters and then fine-tuned online using

Table 9: Results of predictive Kubernetes Horizontal Pod Autoscaling in cold start (transfer forecasting) setting. The source FaaS cluster is selected randomly from history record, and the target cluster is the same as Table 8.

Models	Ave-Lat(s)	Max-Lat(s)	99.9-Lat(s)	99-Lat(s)	90-Lat(s)	AvePod	MaxPod
iTransformer	0.334	97.692	9.331	1.977	0.577	16.291	27
FSNet	0.254	14.338	2.971	1.313	0.424	15.449	33
OneNet	0.269	52.741	3.221	1.232	0.443	15.841	26
Naïve HPA	0.231	91.022	8.275	0.689	0.343	16.574	34
Ideal	0.219	9.419	2.087	0.739	0.371	14.608	24
E ³ Former-FTPL	0.223	12.317	2.311	0.771	0.379	15.229	26
E ³ Former-OS	0.232	15.691	2.396	0.766	0.368	15.393	25

data from the target cluster for cross-data transfer predictions, the results are shown in Table 9.

Due to the lack of historical data, the forecasting errors of the models is often larger at the beginning of online forecasting, which affects the effectiveness of auto-scaling (as evidenced by higher maximum latency and maximum Pod occupations compared to the results in Table 8 for all models). However, thanks to the targeted design of E³Former (including the Adapter and Ensembler), it can adapt more quickly to the dynamic trends of the sequence and produce more robust forecastings. As a result, metrics such as average latency, 90th percentile (p90) latency, and average Pod occupations are comparable to those in Table 8. In particular, E³Former-FTPL achieves results closest to the Ideal HPA strategy, which can be attributed to the simplicity of the FTPL algorithm, which endows it with the better generalizability.

6 CONCLUSION

We design a novel ensemble learning model specifically for the nuanced demands of workload forecasting in large-scale cloud systems. Our model synergizes the predictive capabilities of multiple subnets based on a shared backbone, thus ensuring superior accuracy in online scenarios, especially in cold starts. Remarkably, it accomplishes this with a minimal increase in computational overhead, adhering to the lean operational ethos of serverless systems. To validate the effectiveness of the model, we have collected a workload dataset of large-scale cloud computing system and open-sourced it to advance community research. Through extensive experimentation on the real-world datasets, we establish the efficacy of our ensemble model. Currently, our method has been deployed within ByteDance’s IHPA platform, which supports the stable operation of over 30 applications, such as Douyin E-Commerce and Toutiao. The predictive auto-scaling capacity reaching over 600,000 CPU cores. On the basis of essentially ensuring service quality, the predictive auto-scaling system can reduce resource utilization by over 40%. In the future, we plan to explore more efficient and accurate predictive auto-scaling systems to support the efficient and lean operation of increasingly large-scale computing and storage tasks.

⁶<https://docs.aws.amazon.com/AmazonECS/latest/developerguide/predictive-auto-scaling.html>

⁷<https://cloud.google.com/compute/docs/autoscaler/predictive-autoscaling>

⁸<https://techcommunity.microsoft.com/blog/azureobservabilityblog/general-availability-predictive-autoscaling-for-vmss/3652844>

⁹<https://help.aliyun.com/zh/ack/serverless-kubernetes/user-guide/deploy-ahpa?spm=a2c4g.11186623.0.0.27197c8dzSnS17>

REFERENCES

- [1] Yanal Alahmad, Tariq Daradkeh, and Anjali Agarwal. 2021. Proactive failure-aware task scheduling framework for cloud computing. *IEEE Access* 9 (2021), 106152–106168.
- [2] Shivani Arbat, Vinodh Kumaran Jayakumar, Jaewoo Lee, Wei Wang, and In Kee Kim. 2022. Wasserstein Adversarial Transformer for Cloud Workload Prediction. In *Conference on Artificial Intelligence (AAAI)*. 12433–12439.
- [3] Ioana Baldini, Paul Castro, Kerry Chang, Perry Cheng, Stephen Fink, Vatche Ishakian, Nick Mitchell, Vinod Muthusamy, Rodric Rabbah, Aleksander Slominski, et al. 2017. Serverless computing: Current trends and open problems. *Research advances in cloud computing* (2017), 1–20.
- [4] Avrim Blum and Yishay Mansour. 2007. From external to internal regret. *Journal of Machine Learning Research* 8, 6 (2007).
- [5] Rodrigo N Calheiros, Enayat Masoumi, Rajiv Ranjan, and Rajkumar Buyya. 2014. Workload Prediction Using ARIMA Model and Its Impact on Cloud Applications' QoS. *IEEE Transactions on Cloud Computing (TCC)* 3, 4 (2014), 449–458.
- [6] Nicolo Cesa-Bianchi and Gábor Lugosi. 2006. *Prediction, learning, and games*. Cambridge university press.
- [7] Jiadong Chen, Yang Luo, Xiuqi Huang, Fuxin Jiang, Yangguang Shi, Tieying Zhang, and Xiaofeng Gao. 2023. IPOC: An Adaptive Interval Prediction Model based on Online Chasing and Conformal Inference for Large-Scale Systems. In *ACM SIGKDD Conference on Knowledge Discovery and Data Mining (SIGKDD)*. 202–212.
- [8] Mincheng Chen, Jingling Yuan, Dongling Liu, and Tao Li. 2020. An Adaption Scheduling Based on Dynamic Weighted Random Forests for Load Demand Forecasting. *Journal of Supercomputing (TJSC)* 76, 3 (2020), 1735–1753.
- [9] Robert B Cleveland, William S Cleveland, Jean E McRae, Irma Terpenning, et al. 1990. STL: A seasonal-trend decomposition. *J. off. Stat* 6, 1 (1990), 3–73.
- [10] Sudipto Das, Feng Li, Vivek R Narasayya, and Arnd Christian König. 2016. Automated Demand-driven Resource Scaling in Relational Database-as-a-service. In *ACM International Conference on Management of Data (SIGMOD)*. 1923–1934.
- [11] Yuaning Gao, Xiuqi Huang, Xuanhe Zhou, Xiaofeng Gao, Guoliang Li, and Guihai Chen. 2023. DBAugur: An Adversarial-based Trend Forecasting System for Diversified Workloads. In *International Conference on Data Engineering (ICDE)*. 1–13.
- [12] Udaya Ghai, Elad Hazan, and Yoram Singer. 2020. Exponentiated gradient meets gradient descent. In *Algorithmic learning theory*. PMLR, 386–407.
- [13] Yunda Guo, Jiak Ge, Panfeng Guo, Yunpeng Chai, Tao Li, Mengnan Shi, Yang Tu, and Jian Ouyang. 2024. PASS: Predictive Auto-Scaling System for Large-scale Enterprise Web Applications. In *ACM Web Conference (WWW)*. 2747–2758.
- [14] Haitian Hang, Xiu Tang, Jianling Sun, Lingfeng Bao, David Lo, and Haoze Wang. 2024. Robust Auto-Scaling with Probabilistic Workload Forecasting for Cloud Databases. In *IEEE International Conference on Data Engineering (ICDE)*. 4016–4029.
- [15] Marton Havasi, Rodolphe Jenatton, Stanislav Fort, Jeremiah Zhe Liu, Jasper Snoek, Balaji Lakshminarayanan, Andrew Mingbo Dai, and Dustin Tran. 2021. Training independent subnetworks for robust prediction. In *International Conference on Learning Representations (ICLR)*.
- [16] Xiao He, Ye Li, Jian Tan, Bin Wu, and Feifei Li. 2023. OneShotSTL: One-Shot Seasonal-Trend Decomposition For Online Time Series Anomaly Detection And Forecasting. *The VLDB Endowment (VLDB)* 16, 6 (2023), 1399–1412.
- [17] Antony S Higginson, Mihaela Dedi, Octavian Arsene, Norman W Paton, and Suzanne M Embury. 2020. Database Workload Capacity Planning Using Time Series Analysis and Machine Learning. In *ACM International Conference on Management of Data (SIGMOD)*. 769–783.
- [18] Steven CH Hoi, Doyen Sahoo, Jing Lu, and Peilin Zhao. 2021. Online Learning: A Comprehensive Survey. *NeuroComputing* 459 (2021), 249–289.
- [19] Charles C Holt. 2004. Forecasting seasonals and trends by exponentially weighted moving averages. *International journal of forecasting* 20, 1 (2004), 5–10.
- [20] Sergey Ioffe and Christian Szegedy. 2015. Batch normalization: Accelerating deep network training by reducing internal covariate shift. In *International conference on machine learning (ICML)*. 448–456.
- [21] Vinodh Kumaran Jayakumar, Jaewoo Lee, In Kee Kim, and Wei Wang. 2020. A Self-Optimized Generic Workload Prediction Framework for Cloud Computing. In *International Parallel and Distributed Processing Symposium (IPDPS)*. IEEE, 779–788.
- [22] Adam Kalai and Santosh Vempala. 2005. Efficient algorithms for online decision problems. *J. Comput. System Sci.* 71, 3 (2005), 291–307.
- [23] Taesung Kim, Jinhee Kim, Yunwon Tae, Cheonbok Park, Jang-Ho Choi, and Jaegul Choo. 2022. Reversible instance normalization for accurate time-series forecasting against distribution shift. In *International Conference on Learning Representations (ICLR)*.
- [24] Jyrki Kivinen and Manfred K Warmuth. 1997. Exponentiated gradient versus gradient descent for linear predictors. *information and computation* 132, 1 (1997), 1–63.
- [25] Wei Li, Jiachi Zhang, Ye Yin, Yan Li, Zhanyang Zhu, Wenchao Zhou, Liang Lin, and Feifei Li. 2024. Flux: Decoupled Auto-Scaling for Heterogeneous Query Workload in Alibaba AnalyticDB. In *Companion of the 2024 International Conference on Management of Data*. 255–268.
- [26] Yong Liu, Tengge Hu, Haoran Zhang, Haixu Wu, Shiyu Wang, Lintao Ma, and Mingsheng Long. 2024. iTransformer: Inverted Transformers Are Effective for Time Series Forecasting. In *International Conference on Learning Representations (ICLR)*.
- [27] Ilya Loshchilov and Frank Hutter. 2019. Decoupled Weight Decay Regularization. In *International Conference on Learning Representations (ICLR)*.
- [28] Lin Ma, Dana Van Aken, Ahmed Hefny, Gustavo Mezerhane, Andrew Pavlo, and Geoffrey J Gordon. 2018. Query-Based Workload Forecasting for Self-Driving Database Management Systems. In *ACM International Conference on Management of Data (SIGMOD)*. 631–645.
- [29] Yuqi Nie, Nam H Nguyen, Phanwadee Sinthong, and Jayant Kalagnanam. 2023. A Time Series is Worth 64 Words: Long-term Forecasting with Transformers. <https://github.com/yuqinie98/PatchTST>. In *International Conference on Learning Representations (ICLR)*.
- [30] Quang Pham, Chenghao Liu, Doyen Sahoo, and Steven Hoi. 2023. Learning Fast and Slow for Online Time Series Forecasting. <https://github.com/salesforce/fsnet>. In *International Conference on Learning Representations (ICLR)*.
- [31] Olga Poppe, Tayo Amunike, Dalitso Banda, Aritra De, Ari Green, Manon Knoetzer, Ehi Nosakhare, Karthik Rajendran, Deepak Shankargouda, Meina Wang, Alan Au, Carlo Curino, Qun Guo, Alekh Jindal, Ajay Kalhan, Morgan Oslake, Sonia Parchani, Vijay Ramani, Raj Sellappan, Saikat Sen, Sheetal Shrotri, Soundararajan Srinivasan, Ping Xia, Shize Xu, Alicia Yang, and Yiwen Zhu. 2020. Seagull: An Infrastructure for Load Prediction and Optimized Resource Allocation. *The VLDB Endowment (VLDB)* 14, 2 (2020), 154–162.
- [32] Olga Poppe, Qun Guo, Willis Lang, Pankaj Arora, Morgan Oslake, Shize Xu, and Ajay Kalhan. 2022. Moneyball: proactive auto-scaling in Microsoft Azure SQL database serverless. *VLDB Endowment* 15, 6 (2022), 1279–1287.
- [33] Chenhao Qu, Rodrigo N Calheiros, and Rajkumar Buyya. 2018. Auto-scaling web applications in clouds: A taxonomy and survey. *ACM Computing Surveys (CSUR)* 51, 4 (2018), 1–33.
- [34] Arun Sai Suggala and Praneeth Netrapalli. 2020. Online non-convex learning: Following the perturbed leader is optimal. In *Algorithmic Learning Theory*. PMLR, 845–861.
- [35] Qingsong Wen, Weiqi Chen, Liang Sun, Zhang Zhang, Liang Wang, Rong Jin, Tieniu Tan, et al. 2024. <https://github.com/yfzhang114/OneNet>. In Onenet: Enhancing time series forecasting models under concept drift by online ensembling. *Advances in Neural Information Processing Systems (NeurIPS)* 36.
- [36] Billy M Williams and Lester A Hoel. 2003. Modeling and forecasting vehicular traffic flow as a seasonal ARIMA process: Theoretical basis and empirical results. *Journal of transportation engineering* 129, 6 (2003), 664–672.
- [37] Gerald Woo, Chenghao Liu, Akshat Kumar, Caiming Xiong, Silvio Savarese, and Doyen Sahoo. 2024. Unified Training of Universal Time Series Forecasting Transformers. In *International Conference on Machine Learning (ICML)*.
- [38] Haixu Wu, Tengge Hu, Yong Liu, Hang Zhou, Jianmin Wang, and Mingsheng Long. 2023. TimesNet: Temporal 2D-Variation Modeling for General Time Series Analysis. <https://github.com/thuml/TimesNet>. In *International Conference on Learning Representations (ICLR)*.
- [39] Haiyan Yin, Ping Li, et al. 2021. Mitigating forgetting in online continual learning with neuron calibration. *Advances in Neural Information Processing Systems* 34 (2021), 10260–10272.
- [40] Ailing Zeng, Muxi Chen, Lei Zhang, and Qiang Xu. 2023. Are transformers effective for time series forecasting?. <https://github.com/cure-lab/LTSF-Linear>. In *AAAI conference on artificial intelligence (AAAI)*, Vol. 37. 11121–11128.
- [41] Lifan Zhao and Yanyan Shen. 2024. Proactive Model Adaptation Against Concept Drift for Online Time Series Forecasting. *arXiv preprint arXiv:2412.08435* (2024).
- [42] Haoyi Zhou, Jianxin Li, Shanghang Zhang, Shuai Zhang, Mengyi Yan, and Hui Xiong. 2023. Expanding the prediction capacity in long sequence time-series forecasting. *Artificial Intelligence (AIJ)* 318 (2023), 103886.
- [43] Tian Zhou, Peisong Niu, Liang Sun, Rong Jin, et al. 2023. One fits all: Power general time series analysis by pretrained lm. *Advances in neural information processing systems* 36 (2023), 43322–43355.
- [44] Zhiqiang Zhou, Chaoli Zhang, Lingna Ma, Jing Gu, Huajie Qian, Qingsong Wen, Liang Sun, Peng Li, and Zhimin Tang. 2023. AHPA: adaptive horizontal pod autoscaling systems on alibaba cloud container service for kubernetes. In *AAAI conference on artificial intelligence (AAAI)*, Vol. 37. 15621–15629.